# Supporting Information

## MXene-Encapsulated Hollow Fe₃O₄ Nanochains Embedded in N-Doped Carbon Nanofibers with Dual Electronic Pathways as Flexible Anodes for High-Performance Li-Ion Batteries

Ying Guo,[a,1] Deyang Zhang,[a,c,1*] Ya Yang,[a] Yangbo Wang,[a] Zuxue Bai,[a] Paul K. Chu,[c] and Yongsong Luo[a,b*]

[a] Key Laboratory of Microelectronics and Energy of Henan Province, Henan Joint International Research Laboratory of New Energy Storage Technology, Xinyang Normal University, Xinyang 464000, P. R. China.

[b] College of Physics and Electronic Engineering, Nanyang Normal University, Nanyang 473061, China.

[c] Department of Physics, Department of Materials Science & Engineering, and Department of Biomedical Engineering, City University of Hong Kong, Tat Chee Avenue, Kowloon, Hong Kong, China.

* Corresponding author. Tel. /fax: +86 376 6391760, E-mail: ysluo@xynu.edu.cn (Y. S. Luo), zdy@xynu.edu.cn (D. Y. Zhang).
[1] These authors contributed equally to this work.

# 1. Experimental Details

## 1.1 Materials

Ethanediol ($\geq$ 99.0%), iron chloride hexahydrate ($FeCl_3 \cdot 6H_2O$, 99%), sodium acetate ($C_2H_3NaO_2$, $\geq$99.0%), N, N-dimethyl formamide (DMF, 99.9%), and polyacrylonitrile (PAN, Mw = 150,000) were purchased from Aladdin. All reagents are of analytical grade and used without further purification.

## 1.2 Synthesis of $Ti_3C_2T_x$ MXene

The $Ti_3AlC_2$ MAX phase was synthesized by spark plasma sintering system (Model: SPS-211HF). The starting powders (TiC, Ti, and Al powders with molar ratios of 1.8 : 1.2 : 1.2) were mixed, ground for 12h, put into a mold with an inner diameter of 15mm, and sintered at 1400 °C for 12 min at a pressure of 30 MPa. The product was ground and sieved through a 400 mesh sieve to produce powders with a particle size less than 35 μm. To accurately etch Al from $Ti_3AlC_2$, 2 g of $Ti_3AlC_2$ powders were slowly added to 70 mL of the etching solution containing 60 mL of 9 M HCl, 10 mL of 49% HF, and 1 g LiF. The mixture was maintained at 35 ºC under agitation for 12 h. The multilayer $Ti_3C_2T_x$ MXene was washed repeatedly with deionized water by centrifugation at 5000 rpm until the pH $\geq$ 6. Next, $Ti_3C_2T_x$ MXene solution was transferred to a special bottle shaking by hand for an hour and then sonicated in the Ar atmosphere for an hour. The solution was washed repeatedly with deionized water by centrifugation at 4000 rpm and the product was collected. To use the product for electrospinning, the solvent (deionized water) was exchanged with

dimethylformamide (DMF) by repeated centrifugation (five times) at 10000 rpm and the DMF solution of $Ti_3C_2T_x$ MXene with a concentration of about 40 mg mL$^{-1}$ was obtained.

## 1.3 Synthesis of Hollow $Fe_3O_4$ Nanospheres

The hollow nanospheres were synthesized by a solvothermal method. In brief, 7.20 g of $FeCl_3 \cdot 6H_2O$ and 20.0 g of sodium acetate were dissolved in 200 mL of ethylene glycol under magnetic stirring. After stirring for 1 h, the resulting homogeneous yellow solution was transferred to a Teflon-lined stainless-steel autoclave. The autoclave was heated at 200 °C for 8 h and then naturally cooled to ambient temperature. Finally, the resulting hollow $Fe_3O_4$ nanospheres were washed several times with ethanol and deionized water and freeze-dried overnight in a lyophilizer.

## 1.4 Synthesis of $Fe_3O_4$@MXene/CNFs

$Fe_3O_4$@MXene/CNFs was synthesized by electrospinning and then stepwise annealing. 1 g of the PDDA-modified hollow $Fe_3O_4$ was dispersed in 5mL of $Ti_3C_2$ solution and mechanically sonicated for 60 min in an ice bath. 0.5 g of PAN were added and stirred continuously overnight. The electrospinning solution was loaded into a 5 mL plastic syringe equipped with an 18 G blunt-tip needle. A positive voltage (20 kV) was applied to the needle tip and a copper collector roller covered with an aluminum foil was grounded. The distance between the needle tip and the collector

was 15 cm and the infusion rate of the solution was controlled to be 1.2 mL h$^{-1}$. The samples were electrospun at a relative humidity below 30%. The electrospun mats were first stabilized in air at 280 °C for 1 h at a ramping rate of 5 °C min$^{-1}$ and then carbonized under argon at a ramping rate of 2 °C min$^{-1}$ at 800 °C for up to 3 h.

## 1.5 Synthesis of MXene/CNFs and Fe$_3$O$_4$/CNFs

For comparison, MXene/CNFs and Fe$_3$O$_4$/CN+Fs were prepared. The control sample of Fe$_3$O$_4$/CNFs (without hollow Fe$_3$O$_4$) was prepared in the same way as Fe$_3$O$_4$@MXene/CNFs but without addition of hollow Fe$_3$O$_4$. Similarly, Fe$_3$O$_4$/CNFs was prepared without adding Ti$_3$C$_2$T$_x$ MXene.

## 1.6 Materials characterization

The crystalline structure and phase of the composites were identified by X-ray diffraction (XRD, Bruker D2 PHASER) using Cu-K$\alpha$ ($\lambda$=1.5418 Å) radiation at 40 kV and 40 mA, with 2$\theta$ between 5° and 80° at room temperature. Raman spectroscopy was carried out using an INVIA Raman microprobe (Renishaw Instruments) with a 532 nm laser source, a 50× objective lens and the laser power is 5%. The chemical elements were analyzed on an X-ray photoelectron spectroscopy (XPS, K-ALPHA 0.5 eV) with a resolution of 0.3-0.5 eV from a monochromated aluminum anode X-ray source. The zeta potential ($\zeta$, mV) values of different samples were measured by a Malvern Zetasizer Nano ZSE analyzer on the basis of the principle of electrophoresis light scattering light scattering. The light source is a

helium-neon solid light source with a wavelength of 633 nm. The thermogravimetric (TG) analyzer curve was performed using an STA449F5 (NETZSCH) with 100 mL min$^{-1}$ of oxygen flow from 20 ℃ to 800 ℃ at a heating rate of 10 ℃ min$^{-1}$. The morphologies were examined on a field emission scanning electron microscope (SEM, Hitachi S-4800), a transmission electron microscope (TEM, FEI Tecnai G2 F20) and an atomic force microscopy (AFM, Bruker Dimension Icon). The elemental analysis was carried out using an energy-dispersive X-ray spectroscope (EDS, Bruker-QUANTAX) attached to the TEM.

## 1.7 Electrochemical evaluation

The electrochemical measurements were conducted using CR2032-type coin cells assembled in an argon-filled glove box with water and oxygen contents below 0.1 ppm. The as-synthesized $Fe_3O_4$@MXene/CNFs membrane was cut into free-standing electrodes with a diameter of 16 mm and a thickness of 0.2 mm (The mass of a single electrode is about 0.0040 g, the area is 2 cm$^2$, and the mass per unit area is 2 mg cm$^2$), dried in a vacuum oven at 80 ℃ overnight, and directly assembled into Li-ion batteries. Neither a metal current collector nor any additives (e.g., conductive carbon or binder) was required. In the lithium ion batteries, Li metal was used as the counter and reference electrode and microporous Celgard 2400 membrane was used as the separator. The electrolyte was composed of a solution of 1 mol L$^{-1}$ $LiPF_6$ dissolved in a mixture of ethyl carbonate and dimethyl carbonate (1/1; v/v) with the addition of 5 wt% fluoroethylene carbonate. Cyclic voltammetry (CV) was carried out on a VMP3

electrochemical workstation under different scanning speed. The electrochemical impedance spectroscopy (EIS) was performed by applying a sine wave with an amplitude of 0.5 mV over the frequency range of 0.01 Hz-100 kHz. Galvanostatic charging-discharging tests were performed on a Neware battery testing system in the potential range of 0.01-3.0 V at room temperature. The specific capacity and area capacity are calculated by normalizing the mass loading and area of $Fe_3O_4$@MXene/CNFs electrode, respectively. MXene/CNFs and $Fe_3O_4$/CNFs were also made into self-standing electrodes for the same test.

## 1.8 Computational details

The magnetite $Fe_3O_4$ nanospheres have an "inverse spinel" structure in which $Fe^{2+}$ atoms occupy half of the octahedral sites and $Fe^{3+}$ atoms are located at both the octahedral and tetrahedral sub-lattices. The experimentally determined lattice parameter of the $Fe_3O_4$ nanospheres (a = 8.396 Å) was used in the simulation[1]. The (111) plane was adopted in the simulation model because it is one of the prominent planes revealed from previous calculation and often exposed in natural and synthetic $Fe_3O_4$ crystals. Here, a 2×2 supercell corresponds to a lattice of 11.873 Å along the directions parallel to the surface. Accordingly, a 4×4 supercell of MXene that has a comparable lattice of 12.300 Å was adopted in the simulation. The $Fe_3O_4$ (111) surface and a $Ti_3C_2$ monolayer were bridged through the O atom and four Fe layers were considered in the $Fe_3O_4$ slab.

First-principles density functional theory (DFT) calculations were performed

using the projector-augmented wave (PAW) method and the Perdew-Burke-Ernzerhof generalized gradient approximation (PBE-GGA) exchange correlation functional[2]. The plane wave cutoff was set to 450 eV with a Hellmann-Feynman forces convergence criterion set to be lower than 0.01 eV $\mathring{A}^{-1}$ during the geometrical optimization. The energy was optimized until the difference between two steps less than $10^{-5}$ eV. Both structures are separately optimized before combination. The van der Waals interaction was considered by adopting the dispersion correction by virtue of DFT-D2 approach. The vacuum space of 20 $\mathring{A}$ at least was selected to avoid the interactions between images. The Brillouin zone was sampled using $2 \times 2 \times 1$ k-meshes for the optimization of atomic structures. Meanwhile, spin-polarized calculations were performed. To analyze interactions between Li and $Fe_3O_4$/CNFs, MXene/CNFs or $Fe_3O_4$@MXene/CNFs, the adsorption energies have been estimated by the following equation:

$$E_a = E_{s+Li} - E_s - E_{Li}$$

Where $E_a$ is the adsorption energy, $E_{s+Li}$ stands for the total adsorption energy of structure, $E_s$ is the total energy of $Fe_3O_4$/CNFs, MXene/CNFs or $Fe_3O_4$@MXene/CNFs, and $E_{Li}$ represents the total energy of Li.
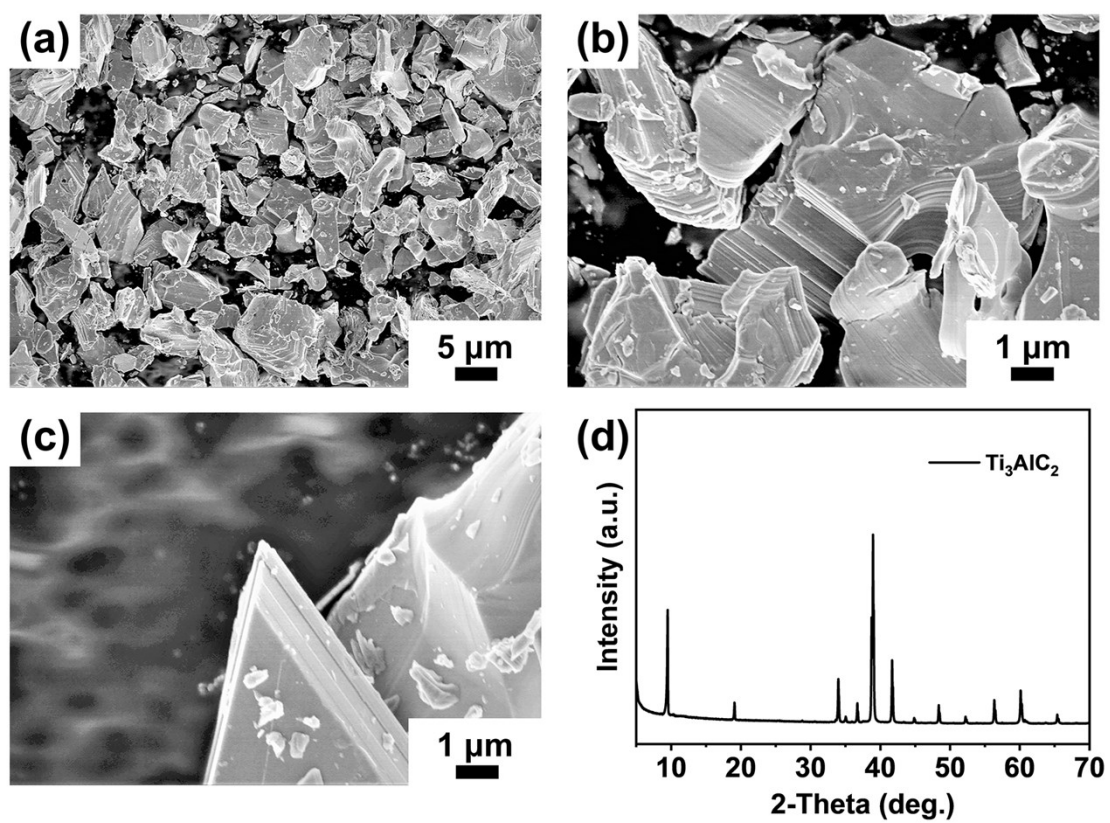
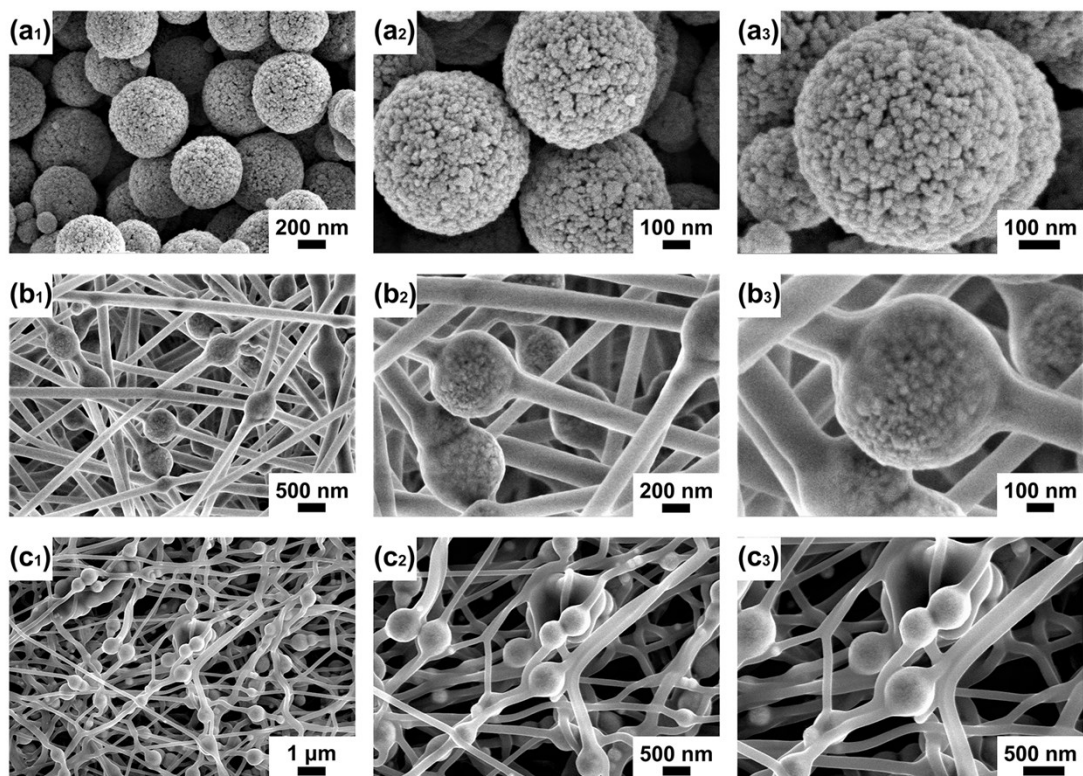**Figure S1.** (a-c) SEM images and (d) XRD pattern of the $Ti_3AlC_2$ powders.

**Figure S2.** ($a_{1-3}$) SEM image of $Fe_3O_4$ nanospheres, ($b_{1-3}$) $Fe_3O_4$/PAN nanofibers, and ($c_{1-3}$) $Fe_3O_4$/CNFs.
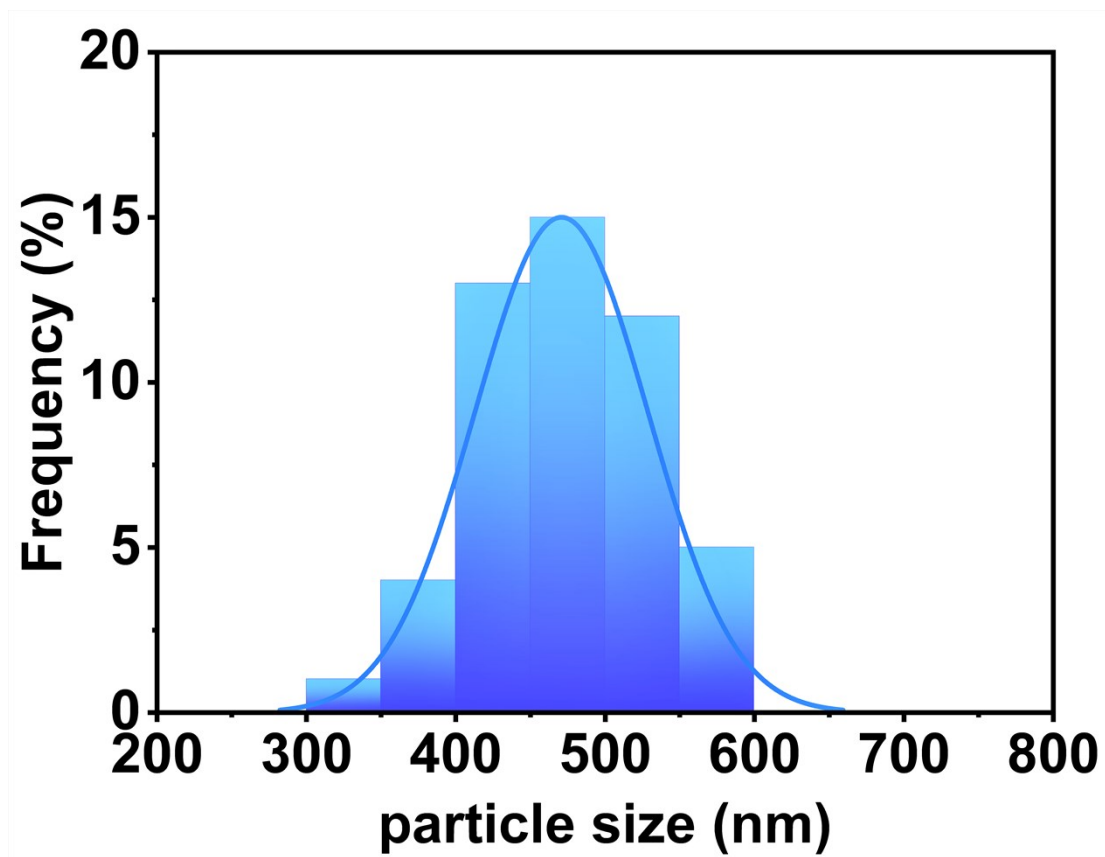
**Figure S3.** Particle size distribution of the $Fe_3O_4$ nanospheres.
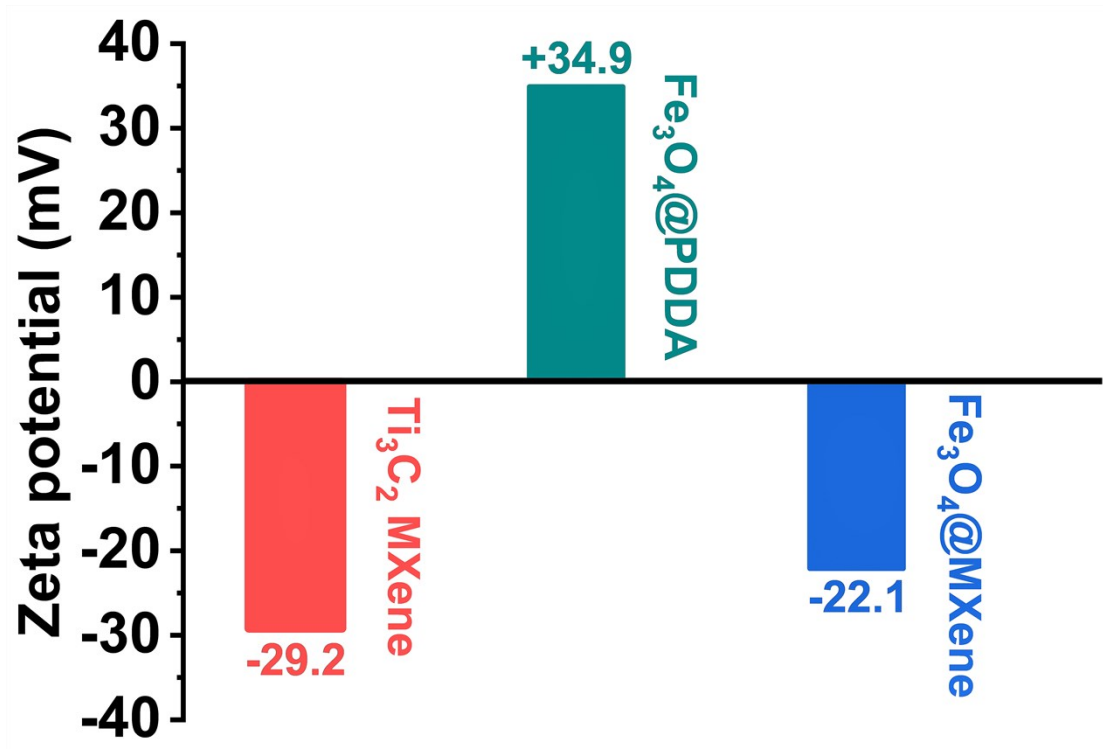
**Figure S4.** Zeta ($\zeta$) potentials of different samples.
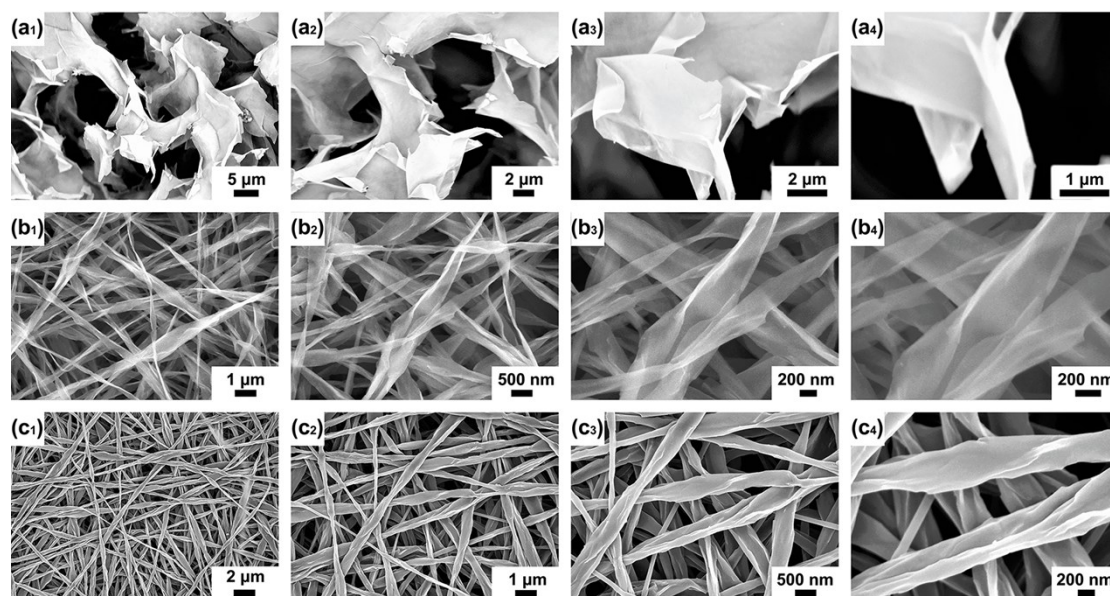
**Figure S5.** (a$_{1-4}$) SEM image of Ti$_3$C$_2$ MXene, (b$_{1-4}$) MXene/PAN nanofibers, and (c$_{1-4}$) MXene/CNFs.
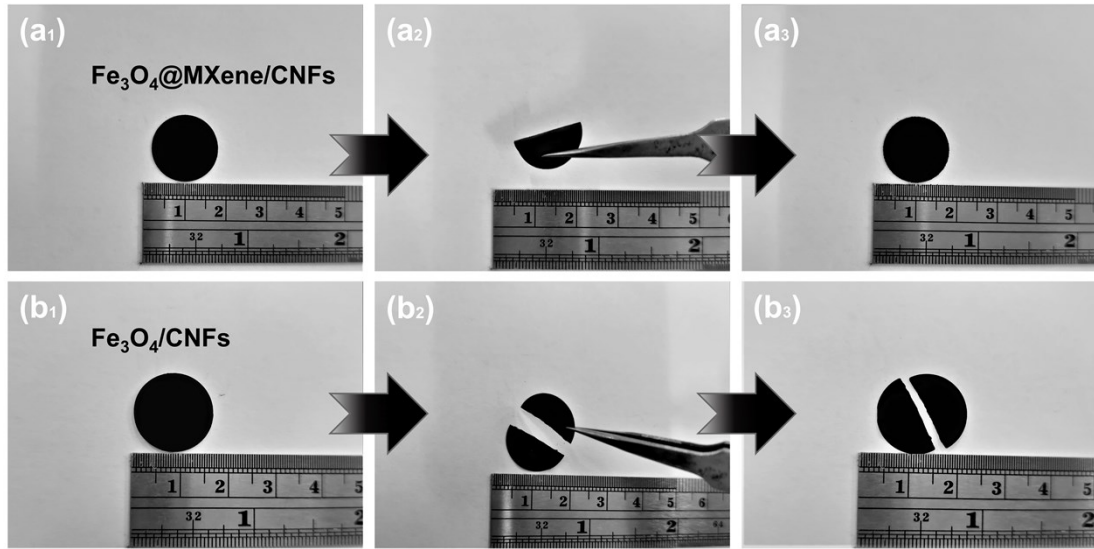
**Figure S6.** Flexibility test of (a$_{1-3}$) Fe$_3$O$_4$@MXene/CNFs and (b$_{1-3}$) Fe$_3$O$_4$/CNFs.
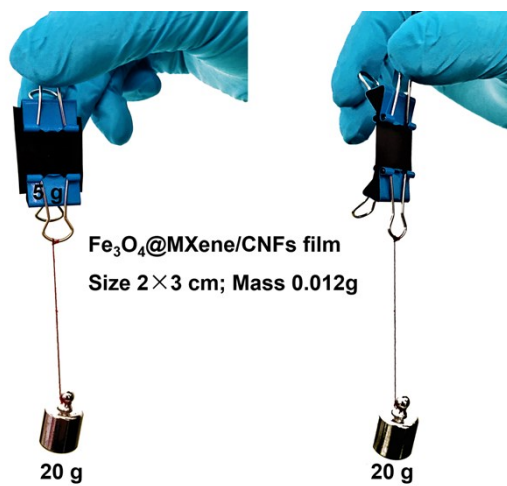
**Figure S7.** Stress-strain test of Fe$_3$O$_4$@MXene/CNFs film.
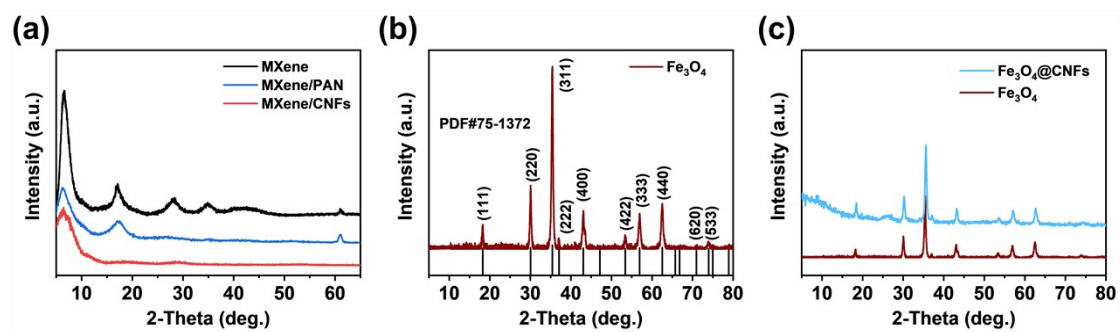
**Figure S8.** XRD patterns of (a) MXene, MXene/PAN nanofibers, and MXene/CNFs, (b) $Fe_3O_4$ nanospheres, and (c) $Fe_3O_4$ and $Fe_3O_4$/CNFs.
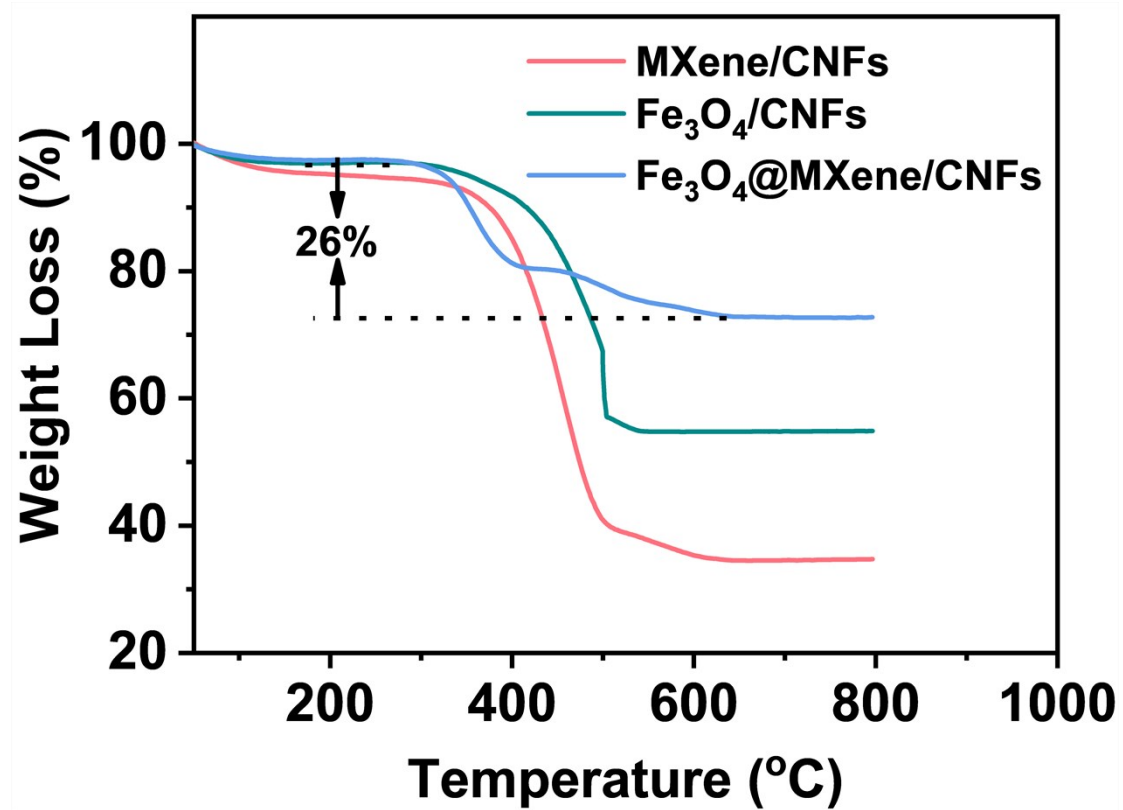
**Figure S9.** TGA curves of MXene/CNFs, $Fe_3O_4$/CNFs, and $Fe_3O_4$@MXene/CNFs.
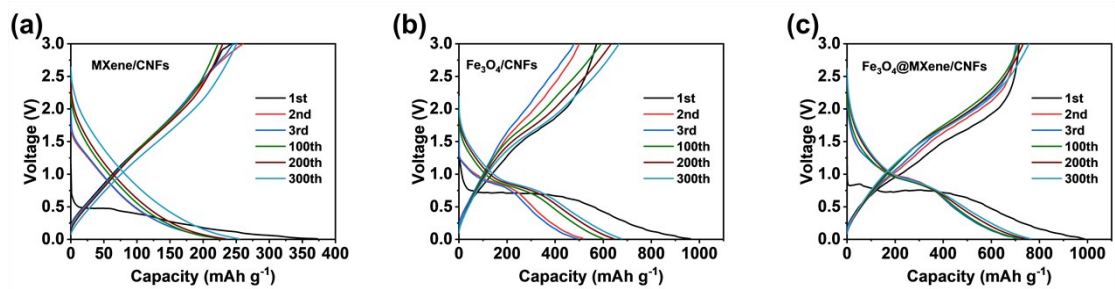
**Figure S10.** Galvanostatic discharge/charge curves of (a) MXene/CNFs, (b) Fe$_3$O$_4$/CNFs, and (c) Fe$_3$O$_4$@MXene/CNFs for various cycles with a current density of 2 A g$^{-1}$.
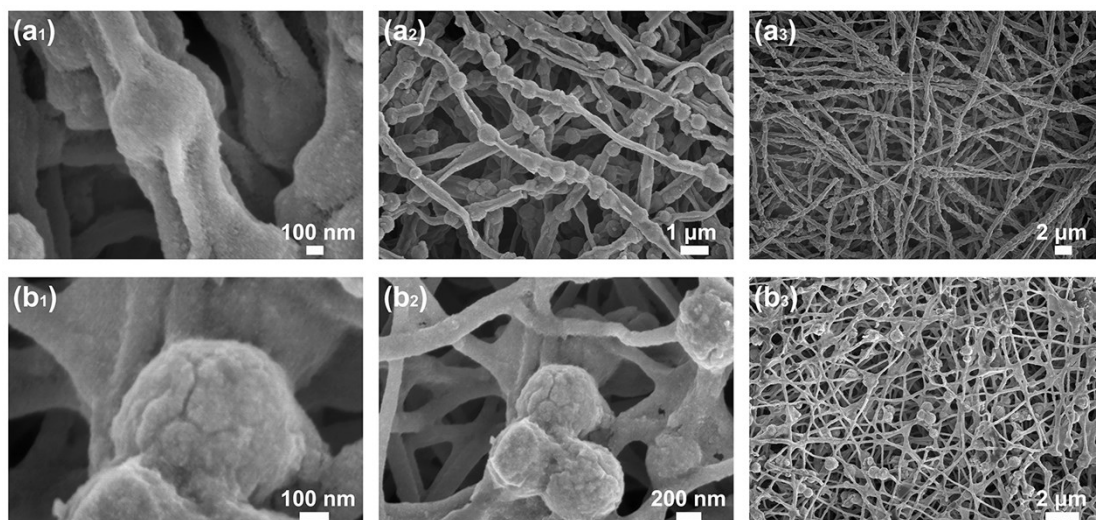
**Figure S11.** SEM image of (a$_{1-3}$) Fe$_3$O$_4$@MXene/CNFs and (b$_{1-3}$) Fe$_3$O$_4$/CNFs after 100 cycles.
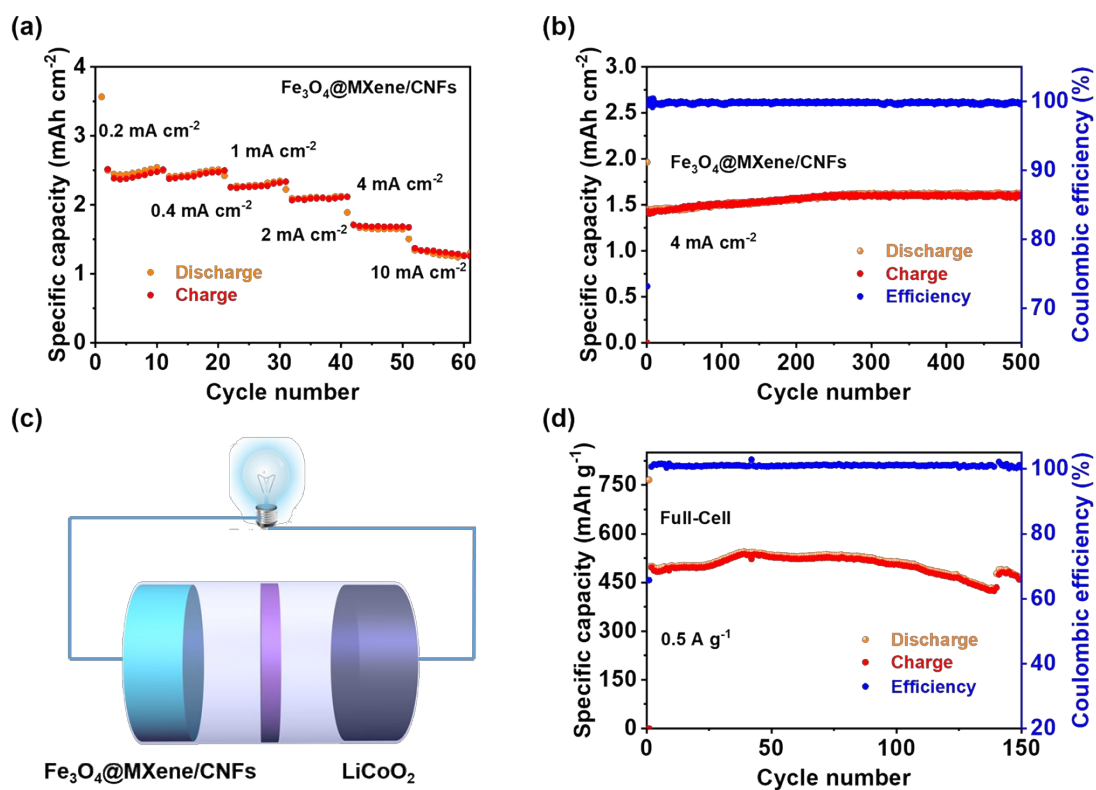
**Figure S12.** (a) The area specific capacities of the Fe$_3$O$_4$@MXene/CNFs anode at different rates (0.2-10 mA cm$^{-2}$); (b) The long cycling performance of self-supported Fe$_3$O$_4$@MXene/CNFs at 4 mA cm$^{-2}$; (c) Schematic diagram of the full-cell with the cathodic LiCoO$_2$ and anodic Fe$_3$O$_4$@MXene/CNFs; (d) Cycling stability of the full-cell at 0.5 A g$^{-1}$.

**Table S1.** Initial discharge capacities and initial coulombic efficiency (CE) of Fe$_3$O$_4$@MXene/CNFs, Fe$_3$O$_4$/CNFs, and MXene/CNFs at 2 A g$^{-1}$.

| Sample | Initial discharge capacity (mAh g$^{-1}$) | Initial coulombic efficiency (%) |
|---|---|---|
| **Fe$_3$O$_4$@MXene/CNFs** | **985.92** | **72.01** |
| Fe$_3$O$_4$@CNFs | 921.44 | 59.88 |
| MXene/CNFs | 373.03 | 62.59 |

**Table S2.** Fitted impedance parameters and equivalent circuit.
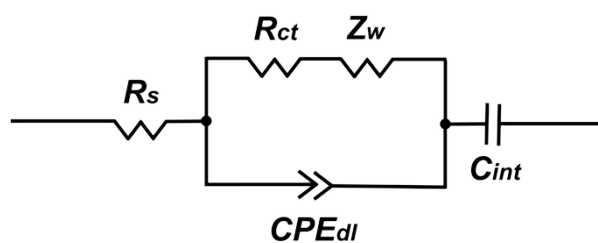


| Sample | $R_s$ (Ω) | $R_{ct}$ (Ω) |
|---|---|---|
| **Fe$_3$O$_4$@MXene/CNFs** | **4.854** | **36.880** |
| Fe$_3$O$_4$@CNFs | 8.540 | 73.432 |
| MXene/CNFs | 3.087 | 17.590 |

**Table S3.** Li ion adsorption ability of MXene/CNFs, $Fe_3O_4$/CNFs, and $Fe_3O_4$@MXene/CNFs.

| Sample | $E_a$ (eV) | $E_{S+Li}$ (eV) | $E_S$ (eV) | $E_{Li}$ (eV) |
|---|---|---|---|---|
| **$Fe_3O_4$@MXene/CNFs** | **-1.86934** | **-1704.9001** | **-1701.13** | **-1.90452** |
| $Fe_3O_4$@CNFs | -0.93636 | -798.49315 | -795.652 | -1.90452 |
| MXene/CNFs | -2.15948 | -252.748 | -248.684 | -1.90452 |

**Table S4.** Capacity retention of the $Fe_3O_4$@MXene/CNFs anode obtained in this work compared with various $Fe_xO_y$-based anode materials as reported in the literature.

| Anode materials | Current density (A g$^{-1}$) | Cycle number | Specific capacity (mAh g$^{-1}$) | Reference |
|---|---|---|---|---|
| $Fe_3O_4$@MXene/CNFs | 2 | 500 | 806 | **This work** |
| $Fe_3O_4$@PPy Nanocages | 2 | 500 | 652 | [3] |
| $Fe_3O_4$@C Nanotubes | 0.5 | 100 | 900 | [4] |
| $Fe_2O_3$/rGO/CNFs | 2 | 400 | 584 | [5] |
| $Fe_3O_4$@$Ti_3C_2$ Hybrids | 0.2 | 100 | 1093 | [6] |
| N-$Ti_3C_2$/$Fe_2O_3$ | 2 | 400 | 549 | [7] |
| N-C@$Fe_3O_4$/rGO | 0.05 | 100 | 900 | [8] |
| $Fe_3O_4$/NCNFs | 0.1 | 200 | 522 | [9] |

# References

1.  J. Han, Q. Fu, B. Xi, X. Ni, C. Yan, J. Feng and S. Xiong, *J. Energy Chem.*, 2021, **52**, 1-11.
2.  W. Yang, J. Zhou, S. Wang, W. Zhang, Z. Wang, F. Lv, K. Wang, Q. Sun and S. Guo, *Energy Environ. Sci.*, 2019, **12**, 1605-1612.
3.  J. Liu, X. Xu, R. Hu, L. Yang and M. Zhu, *Adv. Energy Mater.*, 2016, **6**, 1600256.
4.  X. Xu, J. Shen, F. Li, Z. Wang, D. Zhang, S. Zuo and J. Liu, *Chem. Eur. J.*, 2020, **26**, 14708-14714.
5.  Q. Zhao, J. Liu, X. Li, Z. Xia, Q. Zhang, M. Zhou, W. Tian, M. Wang, H. Hu, Z. Li, W. Wu, H. Ning and M. Wu, *Chem. Eng. J.*, 2019, **369**, 215-222.
6.  D. Xu, K. Ma, L. Chen, Y. Hu, H. Jiang and C. Li, *Chem. Eng. Sci.*, 2020, **212**, 115342.
7.  Z. Zhang, L. Weng, Q. Rao, S. Yang, J. Hu, J. Cai and Y. Min, *J. Power Sources*, 2019, **439**, 227107.
8.  C.-L. Liang, J. Li, Q. Tian, Q. Lin, R.-Y. Bao, Y. Liu, X. Peng, M.-B. Yang and W. Yang, *Ionics*, 2019, **25**, 1513-1521.
9.  L. Guo, H. Sun, C. Qin, W. Li, F. Wang, W. Song, J. Du, F. Zhong and Y. Ding, *Appl. Surf. Sci.*, 2018, **459**, 263-270.